3-2006

Interferometric studies of a piano soundboard

Thomas R. Moore
Department of Physics, Rollins College, TMOORE@rollins.edu

Sarah A. Zietlow
Department of Physics, Rollins College

Published In

Sarah A. Zietlow, and Thomas R. Moore. 2006. Interferometric studies of a piano soundboard. The Journal of the Acoustical Society of America 119 (3): 1783-93.

Interferometric studies of a piano soundboard

Thomas R. Moore and Sarah A. Zietlow
Department of Physics, Rollins College, Winter Park, Florida 32789

(Received 15 June 2005; revised 11 December 2005; accepted 13 December 2005)

Electronic speckle pattern interferometry has been used to study the deflection shapes of a piano soundboard. A design for an interferometer that can image such an unstable object is introduced, and interferograms of a piano soundboard obtained using this interferometer are presented. Deflection shapes are analyzed and compared to a finite-element model, and it is shown that the force the strings exert on the soundboard is important in determining the mode shapes and resonant frequencies. Measurements of resonance frequencies and driving-point impedance made using the interferometer are also presented. © *2006 Acoustical Society of America.*
[DOI: 10.1121/1.2164989]

PACS number(s): 43.75.Mn, 43.40.At, 43.20.Ks [NHF] Pages: 1783–1793

I. INTRODUCTION

A complete understanding of how the dynamics of the modern piano creates its unique sound is unlikely without a thorough understanding of the soundboard. Probably the most important parameter associated with the soundboard is the impedance at the point where the strings meet the bridge, and there are several reports of investigations of the dependence of the driving-point impedance on frequency.[1–6] However, there are parameters beyond the mere value of the impedance at the terminating point of the strings that are important. Of particular interest are the soundboard deflection shapes. These shapes have been reported to be similar to the shapes of the normal modes for frequencies below approximately 200 Hz; above this limit the resonances of the soundboard are believed to be broad and closely spaced so that the deflection shapes do not necessarily resemble the mode shapes.[7,8] Understanding the deflection shapes is important not only because they provide some insight into the physical basis for the impedance structure at the bridge, but also because they can provide insight into effects, such as acoustic short circuiting, which may not affect the driving point impedance but may significantly affect the sound perceived by the listener.

The most common methods for determining the deflection shapes of objects include observing Chladni patterns, measuring the acoustic power as a function of position, making impact measurements, and performing holographic or speckle pattern interferometry. However, each of these techniques is difficult to use in determining the deflection shapes of a piano soundboard.

In principle Chladni patterns are simple to create, but they are extremely difficult to obtain on a fully assembled piano for several reasons. Although some Chladni patterns have been obtained on a soundboard isolated from the piano,[3] the utility of this method is limited by the necessity to physically access the entire soundboard, the requirement that the soundboard be oriented horizontally, and the fact that there are ribs and other attachments that segment the surface.

Recently, acoustic measurements have yielded information on the shapes of the lowest modes of a piano soundboard; however, these measurements have very low spatial resolution.[9,10] Likewise, mechanical measurements of the deflection of a soundboard have been made by physically placing accelerometers on an isolated soundboard as it is struck. This technique is limited by the necessity for physical access to all points of the soundboard, and it is therefore not feasible to perform the measurements on a fully assembled piano. Furthermore, the measurement process can potentially change the resonance structure and the spatial resolution is quite low.[2,7,8,11]

Time-averaged holographic or speckle pattern interferometry both provide interferograms that can reveal the deflection shape of a vibrating object, and both techniques have been used often to determine deflection shapes of musical instruments. However, the size and mass of a fully assembled piano make both types of interferometry a very difficult undertaking. Specifically, these interferometric techniques require extensive vibration isolation. A good estimate of the requirement for vibration isolation is that the movement of the object due to ambient vibrations must be significantly less than one-tenth of the wavelength of the light used to image the object. This stability must be maintained over the entire time it takes to perform the experiment. The high center of mass, large surface area, and wooden construction of a piano make this level of isolation problematic. Even when enclosed within a soundproof room, and mounted on supports with active vibration control mechanisms, vibrations that are transmitted through the support structure usually make such large objects too unstable to be effectively studied using these techniques.

To investigate the deflection shapes of a piano soundboard, we have modified the common form of the speckle pattern interferometer so that ambient vibrations that are difficult to eliminate do not degrade the time-averaged interferogram. In fact, when using this interferometer the decorrelation of the speckle pattern actually increases the precision of the measurements. This modification, combined with a recently reported modification that reduces the complexity of the interferometer while simultaneously reducing the necessary laser power,[12,13] has enabled us to optically investigate the deflection shapes of a fully strung piano soundboard *in situ*.

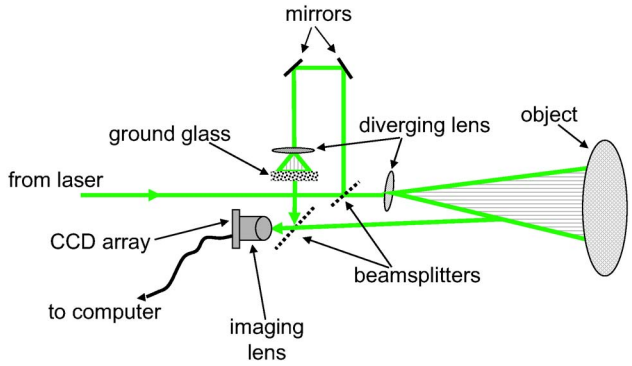

FIG. 1. (Color online) Diagram of the electronic speckle pattern interferometer.

In what follows we describe this interferometer, the theory of its operation, and its application to the study of a piano soundboard. We begin by discussing the most common form of the electronic speckle pattern interferometer and highlight the problems associated with using it to investigate the soundboard. We then describe a modification to the interferometer and present a theory showing that with this modification a slow decorrelation of the speckle pattern enhances the sensitivity. Next, we present some interferograms of the deflection shapes of the soundboard of a fully assembled piano that were made using this method, discuss their implications, and compare interferograms of the lowest modes with finite-element models. Finally, we demonstrate that data obtained using this interferometer can be used to determine the resonance curves of the soundboard, as well as make measurements of the driving-point impedance.

II. THEORY OF TIME-AVERAGED ELECTRONIC SPECKLE PATTERN INTERFEROMETRY WITH DECORRELATION

The arrangement of the electronic speckle pattern interferometer used in our experiments is shown in Fig. 1. It is a modified version of the more common arrangement and a detailed description can be found in Refs. 12 and 13. To create an interferogram, a beam of coherent light is reflected from an object and imaged through a beamsplitter onto a charge-coupled device (CCD) array. A reference beam is directed through a delay leg and illuminates a piece of ground glass, which is also in the view of the imaging lens through reflection from the beamsplitter. To study harmonically vibrating objects, the image present on the CCD array is digitally stored prior to the onset of harmonic motion of the object. Once the object is executing harmonic motion, the image on the array is then subtracted from the initial image in real time.

This situation can be described theoretically by assuming that the object under investigation is moving with simple harmonic motion, with an angular frequency of ω_0 and an amplitude of Δz. Assuming that the size of the speckle is approximately the size of a single pixel element, the intensity of the light on a pixel is given by

$$I = I_r + I_0 + 2\sqrt{I_r I_0}\cos\theta, \tag{1}$$

where I_r and I_0 are the intensities of the reference and object beam, respectively, and

$$\theta = \theta_0 + \xi\sin(\omega_0 t). \tag{2}$$

In this equation

$$\xi = \frac{2\pi\Delta z}{\lambda}(\cos\theta_i + \cos\theta_r), \tag{3}$$

and θ_0 is the initial difference in phases of the two beams at the pixel element. In Eq. (3), θ_i and θ_r represent the incident and reflected angles of the object beam measured from the normal to the surface of the object under study, and λ is the wavelength of the light.

For the case considered here the integration time of the detector is long compared to the period of the motion; therefore, it records only the time-averaged intensity of the interference. Assuming that the intensities of the two beams are constant in time, the recorded intensity is given by

$$\langle I\rangle = I_r + I_0 + 2\sqrt{I_r I_0}\langle\cos[\theta_0 + \xi\sin(\omega_0 t)]\rangle, \tag{4}$$

where the angled brackets indicate a time average. Performing the time average explicitly reduces Eq. (4) to[14]

$$\langle I\rangle = I_r + I_0 + 2\sqrt{I_r I_0}\,J_0(\xi)\cos\theta_0, \tag{5}$$

where J_0 represents the zero-order Bessel function of the first kind.

The most common method of viewing the amplitude of displacement is to record an initial image before the onset of vibration of the object and subtract it from an image recorded subsequent to the onset of harmonic motion; the absolute value of the difference is then displayed on a computer monitor. In this case the intensity recorded by the first frame is given by

$$I_1 = I_r + I_0 + 2\sqrt{I_r I_0}\cos\theta_0, \tag{6}$$

and the intensity recorded after the onset of vibration of the object is given by Eq. (5). When the two are subtracted, the intensity of the pixel displayed on the monitor after the nth frame is given by

$$I_n = \beta_n|1 - J_0(\xi)|, \tag{7}$$

where β_n is a positive constant with a value that depends upon the relative intensities of the image and reference beams, as well as the details of the display.

For the interferometer to provide the results indicated by Eq. (7), the object must be stable enough such that the speckle pattern does not decorrelate in the time between obtaining the initial and final image. Therefore, the interferometer and the object under study are typically isolated from ambient vibrations.

When the object under investigation is large or flimsy, adequate isolation from ambient vibrations can become difficult. Any displacement due to motion of the structure upon which the object rests increases linearly with height, and an object with a high center of mass, such as a piano, enhances the effects of any slight motion. Even when the interferometer and the piano sit on tables with active pneumatic vibra-

tion isolation, and the entire apparatus is enclosed within a room without circulating air, we have found that the speckle can decorrelate on a time scale significantly less than 1 second. This decorrelation may occur even more quickly if the interferometer and the object under study are independently supported, which may be required to image large objects such as pianos.

To include the decorrelation due to ambient vibration, an extra term must be added to Eq. (2). While the ambient vibrations may contain many frequencies, it is most difficult to isolate a large object from vibrations with long periods; therefore, we assume that the period of the movement responsible for speckle decorrelation is significantly greater than the period of the oscillation of interest. Under this condition,

$$\theta = \theta_0 + \frac{2\pi}{\lambda}\eta \sin(\sigma t) + \xi \sin(\omega_0 t), \tag{8}$$

where η is the amplitude of the oscillation and it is assumed that $\sigma \ll \omega_0$.

If the integration time of the detector is short compared to σ^{-1}, the small angle approximation may be applied and the movement can be approximated as a slow linear movement over the integration time of the detector. In this case Eq. (8) becomes

$$\theta = \theta_0 + \sigma t + \xi \sin(\omega_0 t). \tag{9}$$

Equation (9) can also be written as

$$\theta = \theta_0 + \varepsilon \omega_0 t + \xi \sin(\omega_0 t), \tag{10}$$

where $\epsilon \ll 1$. If the integration time of the detector is short compared to σ^{-1}, the intensity of the light incident on a pixel of the recording array is given by

$$\langle I_n \rangle = I_r + I_0 + 2\sqrt{I_r I_0}\langle \cos[\theta_0 + \varepsilon \omega_0 t + \xi \sin(\omega_0 t)] \rangle. \tag{11}$$

When integrated, the function within the angled brackets in the above equation is a form of the equation known as Anger's function, which is a generalization of the Bessel function of the first kind.[14] When ϵ is an integer, Anger's function reduces to a Bessel function of order ϵ.

Since we have assumed that $\epsilon \ll 1$, we can approximate the time-averaged term in Eq. (11) as Anger's function with $\epsilon = 0$. In this case Eq. (11) reduces to Eq. (5). However, since the small-angle approximation used to obtain Eq. (10) is not valid for times that are not short compared to σ^{-1}, θ_0 cannot be considered to be constant over long periods of time. That is, although we may assume that ϵ is approximately zero for the purpose of evaluating Eq. (11), any nonzero value of ϵ will result in a time-varying value of θ_0 that cannot be ignored over time periods that are not short compared to σ^{-1}.

If the time between the collection of images in electronic speckle pattern interferometry is long compared to σ^{-1}, and the integration time of the detector is short compared to this value, subtracting the pixel value recorded after the onset of vibration from the value of the same pixel recorded before the onset of vibration will generally provide a nonzero result. This nonzero result will occur even when the object has not been intentionally set into motion. Therefore, speckle pattern interferometry yields no usable information about the harmonic movement of the object unless the time between images is short compared to σ^{-1}.

However, when the initial image and the final image are both recorded while the object is oscillating at frequency ω_0, rather than the initial frame being recorded prior to the onset of vibration, Eq. (11) describes the intensity of both images. Under these circumstances the intensity shown on the computer monitor is proportional to the absolute value of the difference between the pixel values in the mth and nth images, i.e.,

$$I_{mn} = \beta_{mn}|J_0(\xi)|, \tag{12}$$

where in this case the value of β_{mn} depends not only upon the details of the monitor settings, but also on the value of the phase angle θ_0, which is slowly varying in time and therefore changes slightly between the mth and nth frames. That is,

$$\beta_{mn} \propto |\cos\theta_m - \cos\theta_n|, \tag{13}$$

where θ_m and θ_n represent the value of the initial phase angle for the mth and nth image, respectively.

If the object is too stable, such that $\cos\theta_m = \cos\theta_n$, the resulting interferogram will be uniformly black and yield no information despite any harmonic movement of the object. In this case it is necessary to subtract an image taken after the onset of vibration from one taken before vibration begins for the interferogram to provide any useful information. Likewise, if the movement that produces the decorrelation is not well approximated by a linear function over the integration time of the detector, then Eq. (12) is not valid.

In the case where there is a slow decorrelation of the light, such that over the integration time of the detector $\cos\theta_m \neq \cos\theta_n$ and $\epsilon \ll 1$, then the brightness of the pixel displayed on the screen will be proportional to $|J_0(\xi)|$, and lines of equal displacement will occur when

$$J_0(\xi) = 0, \tag{14}$$

where ξ is defined by Eq. (3). Averaging over several frames will eliminate the possibility of a spurious result due to $\cos\theta_m$ and $\cos\theta_n$ being equal simply by chance.

Note that Eq. (12) indicates that nodes in the soundboard will appear white on the monitor, while black lines indicate contours of equal amplitude of vibration. In the case where the initial frame is recorded before the onset of harmonic vibration, Eq. (7) indicates that areas of no movement appear as black, while white lines indicate contours of equal amplitude. Note also that the resolution of the system described by Eq. (12) is twice that described by Eq. (7), because Eq. (12) indicates that minima in the interferogram occur at every point where the Bessel function has a value of zero. Equation (7) indicates that minima occur only at the maxima of the Bessel function.

In the case where the object under investigation is stable so that $\cos\theta_m = \cos\theta_n$, a slow linear shift can be added to either the reference beam or the object beam; similarly, a slow physical motion of the object can be induced artificially. Either of these techniques will ensure that ϵ is nonzero but significantly less than unity, and will result in the increased

precision of the interferometer. Yet, precision is seldom the problem when attempting electronic speckle pattern interferometry in the laboratory.

As noted above, large objects such as pianos are normally not stable enough to image using electronic speckle pattern interferometry due to the presence of small ambient motions transmitted through the support structure. However, if the ambient motion is slow compared to the driving frequency ω_0, the motion will decorrelate the speckle within the constraints outlined above. In this case, speckle pattern interferometry can be used to study the motion of these objects. That is, as long as there is some slowly varying motion of the object, even if the motion is caused by ambient vibrations that normally precludes the use of interferometry, useful interferograms can be obtained.

Before concluding this section we note that assuming $\epsilon \sim 0$ ensures that we can approximate the time average in Eq. (11) as a zero-order Bessel function of the first kind. However, this is not a necessary approximation since Eq. (11) can be calculated explicitly for any value of ϵ. Interferograms can be obtained even for large values of ϵ; however, knowledge of its value is necessary to make measurements of the amplitude of the motion. We address this issue further in Sec. IV.

III. EXPERIMENTAL ARRANGEMENT

All of the experiments reported here were performed on a Hallet and Davis piano manufactured circa 1950. The piano was a spinet model, with a soundboard measuring approximately 1.4×0.63 meters. The soundboard was of varying thickness, as is usually the case; however, precise measurements of the thickness were not possible without significantly altering the piano and were therefore not made. The profile of the bottom of the soundboard could be unambiguously measured, and it was found that the thickness varied from 4.4 ± 0.1 to 6.9 ± 0.1 mm.

The soundboard of the piano was made of solid spruce, with the grain direction being 32° from the horizontal, diagonal from the upper left to lower right as viewed from the back of the piano. There were 12 ribs made of pine and glued to the back of the soundboard in an orientation perpendicular to the grain. The ribs had a width of approximately 25 mm, were spaced approximately 80 mm apart, and ranged in length from approximately 217 to 725 mm.

There were two bridges on the front of the soundboard over which the strings passed. A treble bridge, approximately 1.12 m in length was placed diagonally from the lower right to the upper left, as viewed from the back. A bass bridge, approximately 0.37 m long, was attached near the bottom of the soundboard. The edges of the soundboard were sandwiched between the case and retaining timbers, resulting in the edges being strongly clamped. Figure 2 contains a drawing of the soundboard, as viewed from the back, indicating the location of the bridges and orientation of the ribs.

Except where it is explicitly noted below, the piano soundboard remained completely strung and attached to the piano frame. No modification of the structure of the piano was made except that the hammers were removed for easier access to the treble bridge. The strings were all damped in two or three places by weaving strips of cloth between them to ensure that vibrations of the strings in no way affected the soundboard vibrations.

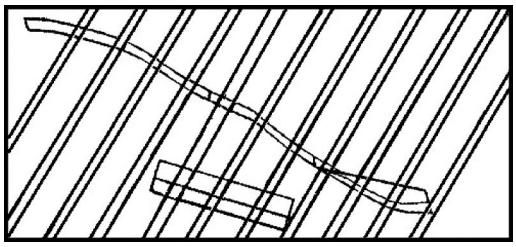

FIG. 2. Drawing of the orientation of the bridges and ribbing of the soundboard as viewed from the back. The bridges are attached to the front of the soundboard and the ribs are attached to the back.

The piano was mounted on an optical table with active pneumatic vibration-isolating legs, and attached to the table with a 3-in. nylon strap. The back of the piano was painted white to efficiently reflect light.

The interferometer was made from discrete optical components mounted on a separate actively isolated optical table. The entire experimental arrangement, with the exception of the laser, was contained within a $10 \times 12 \times 7$ ft. room, which was tiled with anechoic foam on all surfaces except for the portions of the floor that supported the optical tables.

The laser used to illuminate the piano was a frequency-doubled $Nd:YVO_4$ laser with a wavelength of 532 nm and a maximum power of 5 W. It was mounted outside of the anechoic room on an optical table with active pneumatic vibration isolation. The light entered the anechoic room through a small hole in the wall. A commercial CCD camera with a 768×494 pixel array and the standard 30-Hz frame rate was used to record the images. The illuminating beam and the imaging system were oriented perpendicular to the soundboard, so that $\cos \theta_i$ and $\cos \theta_r$ were both very close to unity.

Since the mass of the tables and the piano exceeded 1000 Kg, and the stability required for interferometry restricts the relative movement of the interferometer and piano to less than 50 nm, the floor of the chamber was not made of a suspended wire mesh as is common. Rather, the floor of the chamber was a portion of a concrete slab that comprised the floor of the building. Although the interferometer and the piano were mounted on tables with active vibration isolation, and both were housed in a chamber tiled with anechoic foam, there was a slight independent motion of the two tables at low frequencies. This motion was transmitted to the tables through the floor, with the peak transmissibility occurring at approximately 1 Hz.

Under normal circumstances the motion of the tables decorrelates the speckle and precludes the use of speckle pattern interferometry. However, since the method outlined above requires some decorrelation, the motion of the tables was advantageous. Thus, the technique described above allowed the use of speckle pattern interferometry in a situation in which it is normally impossible.

As outlined in the theory above, an image from the camera was digitally stored after the soundboard was set into

harmonic motion. Each subsequent frame was then digitally subtracted in real time from the previous image. Black lines appeared on the interferogram when the condition set forth in Eq. (14) was met.

During the experiments, vibrations of the soundboard were induced at an angular frequency of ω_0. The two motions, one harmonic with angular frequency ω_0 and one slowly varying so that it appeared linear over the integration time of the detector, were completely independent of one another. The slower vibrations occurred continually, regardless of the presence or absence of the driven harmonic motion.

Since the decorrelation time due to the ambient vibrations was on the order of the integration time of the CCD array, good interferograms were obtained by subtracting contiguous frames, thus allowing real-time viewing of the interferograms. Some higher frequency ambient vibrations resulted in noticeable noise in the interferograms, which was manifest as a series of lines unrelated to the harmonic motion of the piano. To eliminate these effects, and produce unambiguous interferograms for later analysis, up to 200 interferograms were averaged before the image was digitally stored. The total time of data collection for a single image, including postprocessing, was less than 10 s.

To obtain interferograms showing the deflection shapes of a piano soundboard, the apparatus described above was used to study the soundboard as it was driven harmonically. The driving force was provided by a speaker placed approximately 2 m from the soundboard. A high-quality function generator provided a sinusoidal signal, which was subsequently amplified and sent to the speaker. Typical deflections of the soundboard were less than a few wavelengths of the illuminating light (i.e., $\sim 0.1-2\ \mu$m) and required a sound intensity level on the order of 50 dB.

In some cases an electromagnetic shaker was used to drive the soundboard vibrations. The shaker was mounted on an adjustable magnetic base so that the driving mechanism could impinge upon any desired part of the soundboard.

IV. RESULTS AND ANALYSIS

A. Deflection shapes of a piano soundboard

Typical interferograms obtained using the apparatus described above are shown in Fig. 3. Three vertical braces and two carrying handles are visible in the interferograms, in addition to the soundboard and the rectangular frame to which it is mounted. The braces and handles are not physically touching the soundboard.

The interferograms in Fig. 3 show the deflection shapes of the soundboard at three different frequencies ranging from 219 Hz to 2.8 kHz. The total amplitude of the deflection at any point can be determined by counting the lines of equal displacement from a nodal point. Table I lists the displacement from the equilibrium position represented by each contour line.

From observations of the interferograms at frequencies between 60 Hz and 3 kHz, it appears that most of the resonances of the soundboard are broad and overlapping. However, the lower resonances appear to be significantly separated in frequency and therefore amenable to study. This conclusion has also been reached by others.[3,7,8] Interferograms of the deflection shapes of the lowest three resonances of the piano are shown in Figs. 4(a), 5(a), and 6(a). The resonant frequencies are shown in the second column of Table II. The bandwidth of the resonances are on the order of 20 Hz; however, the peak response is easily discerned by viewing the interferograms in real time while changing the driving frequency.

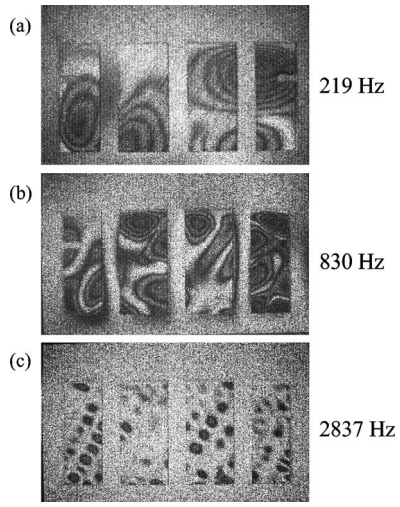

FIG. 3. Interferograms of the soundboard of a spinet piano. The vibrations are driven acoustically from a speaker placed approximately 2 m away.

The simplest model of a piano soundboard is that of an isotropic rectangular plate clamped at the edges. Leissa has reprinted the frequency parameters necessary for finding the resonant frequencies of rectangular plates with several aspect ratios.[15] The frequency parameter is defined as

$$\gamma = 2\pi f a^2 \sqrt{\frac{\rho}{D}}, \tag{15}$$

where f is the resonant frequency, a is the length of the shortest side of the plate, ρ is the area density, and D is the rigidity of the plate, which is defined as

TABLE I. The total amplitude of vibration represented by the number of dark lines traversed from a nodal point in an interferogram. Each line represents a point where Eq. (14) is valid.

Contour	Displacement (nm)
1	102
2	234
3	366
4	499
5	632
6	765
7	898
8	1031
9	1164
10	1297

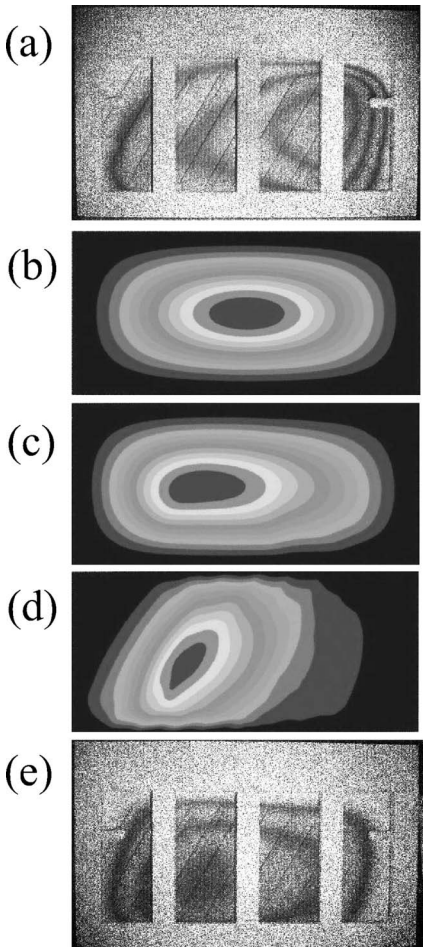

FIG. 4. Deflection shape of the first mode of the piano soundboard (a) observed interferometrically; (b) predicted by finite-element analysis of an isotropic soundboard; (c) predicted by finite-element analysis of an isotropic soundboard with bridges attached; (d) predicted by finite-element analysis of an orthotropic soundboard with ribs and bridges attached; and (e) observed interferometrically with no string tension. The resonant frequencies are listed in Table II.

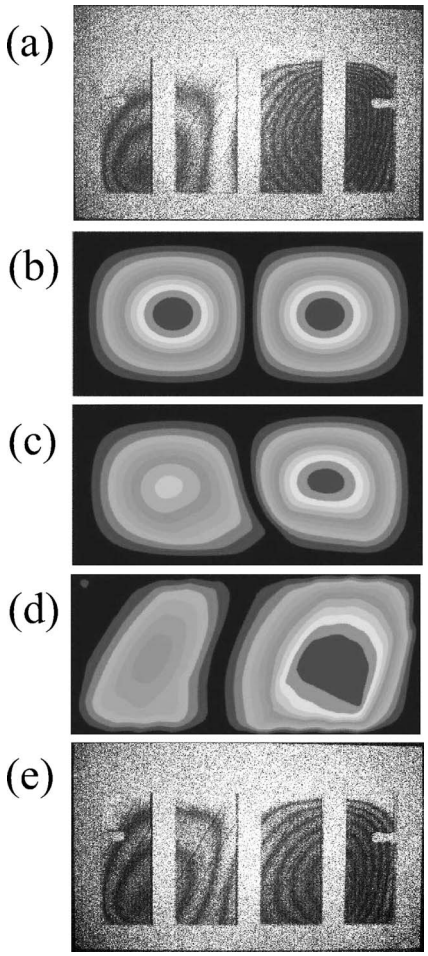

FIG. 5. Deflection shape of the second mode of the piano soundboard (a) observed interferometrically; (b) predicted by finite-element analysis of an isotropic soundboard; (c) predicted by finite-element analysis of an isotropic soundboard with bridges attached; (d) predicted by finite-element analysis of an orthotropic soundboard with ribs and bridges attached; and (e) observed interferometrically with no string tension. The resonant frequencies are listed in Table II.

$$D = \frac{Eh^3}{12(1-\nu^2)}, \tag{16}$$

where E is Young's modulus, h is the thickness of the plate, and ν is Poisson's ratio. Knowing the frequency parameter for any mode uniquely determines the frequency of that mode.

The aspect ratio of this particular soundboard is 0.45, which is very close to the aspect ratio of 0.5, for which the frequency parameters are reported by Leissa derived from work by Bolotin.[16] A good estimate of the correct value of the frequency parameters can be determined from these values by interpolation, which yields frequency parameters of 23.9, 29.9, and 40.7 for the first three modes of the soundboard.

Using Eq. (15), the frequencies of the lowest modes of an isotropic soundboard were calculated. The values for the density, Young's modulus, and Poisson's ratio were taken from the literature; all other parameters were measured.[17] These calculated frequencies are shown in the third column of Table II. This model is adequate to predict the approximate frequencies of the two lowest resonant modes of this soundboard; however, there are significant variances between the observed mode shapes and those of an isotropic rectangular plate clamped at the edges.

An analysis of the mode shapes shown in Figs. 4(a), 5(a), and 6(a) leads one to believe that the soundboard is not modeled well by a simple isotropic rectangular plate clamped at the edges, even though the resonant frequencies of the two lowest modes can be estimated using this model. Since the ribs are oriented in the direction perpendicular to the wood grain of the soundboard, and the spacing between them is much smaller than the wavelengths of the bending waves that are associated with the lowest modes in the wood, the soundboard should present an almost isotropic medium for the lower modes.[2] However, the soundboard under investigation exhibits some large-scale anisotropy, which can be deduced because the antinodes of all of the lowest three modes are noticeably shifted from their expected, symmetric positions.

Since the wavelength of the flexural waves in the soundboard at these low frequencies is on the order of the size of the soundboard, and there are no obvious small-scale aberra-

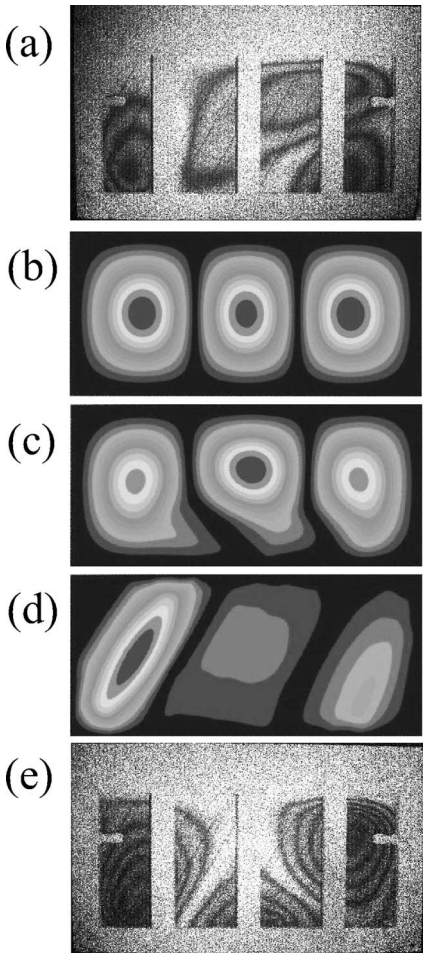

FIG. 6. Deflection shape of the third mode of the piano soundboard (a) observed interferometrically; (b) predicted by finite-element analysis of an isotropic soundboard; (c) predicted by finite-element analysis of an isotropic soundboard with bridges attached; (d) predicted by finite-element analysis of an orthotropic soundboard with ribs and bridges attached; and (e) observed interferometrically with no string tension. The resonant frequencies are listed in Table II.

tions in the mode shapes, it is likely that the cause of the asymmetry in the mode shapes is not due to small asymmetries in the soundboard. Indeed, it is likely that the observed asymmetries of the mode shapes are due to the presence of the bridges.

To test this hypothesis a finite-element model was constructed using a commercially available software program. The soundboard was assumed to be an isotropic board of sitka spruce with a thickness of 5.6 mm, which was the average thickness at the bottom of the actual soundboard. The model had approximately 39 000 elements and the edges were assumed to be clamped. The results of the model are shown in Figs. 4(b), 5(b), and 6(b). The resonant frequencies of the soundboard predicted by this model are found in the fourth column of Table II. As expected, the modes are symmetric and the predicted resonant frequencies are similar to those found analytically.

When the two bridges are added to the model the frequencies of the two lowest resonances change little, but the modal shapes of all three modes change significantly. The resonant frequencies of the soundboard predicted by this model are found in the fifth column of Table II. Figures 4(c), 5(c), and 6(c) show the shapes of the first three modes predicted by this model. Note that the antinodes and the nodal lines are shifted from the positions predicted by the simple model of an isotropic board. However, comparing these predictions with the interferograms shown in Figs. 4(a), 5(a), and 6(a) reveals that these mode shapes do not compare well with the experimental data. In particular, the antinode of the first mode and the nodal line of the second mode are both shifted to the incorrect side of the center of the soundboard. Additionally, the predicted deflection shape of the third mode remains significantly different than the experimentally observed shape.

Despite the poor agreement between the observed and predicted deflection shapes, the frequencies of the modes predicted by this model agree quite well with the observed frequencies. In particular, the addition of the bridges to the model has a significant effect on the frequency of the third mode. However, the large-scale anisotropy of the mode shapes, which does not appear to be accounted for by the presence of the bridges, indicates that it may be necessary to include the orthotropic nature of the wood and the presence of the ribs in the model.

The predictions of the mode shapes from a model that includes the orthotropy of the wood, the ribs, and the bridges are shown in Figs. 4(d), 5(d), and 6(d). The resonant frequencies of the soundboard predicted by this model are found in the sixth column of Table II. Note that the predictions of this model show better agreement with the experimentally observed mode shape of the second mode than the previous model, but the poor agreement between the predictions for the first and third modes remains. Additionally, the predicted frequencies for all modes are significantly changed, showing poor agreement with the experimentally derived values.

From this analysis one may conclude that by adding complexity to the model, and thus making it more similar to the actual piano, the predicted resonant frequencies are

TABLE II. The measured and calculated resonant frequencies (in Hz) of the soundboard. See the text for details.

Mode	Measured (±1 Hz)	Analytical	FEA isotropic	FEA isotropic with bridges	FEA orthotropic with ribs and bridges	Measured without strings (±1 Hz)
1	112	93	99	92	74	80
2	129	116	123	126	90	110
3	204	158	168	198	101	170

shifted further from the actual frequencies. Furthermore, the mode shapes predicted by the model are significantly different from those observed experimentally.

The poor agreement between the model and the interferograms leads one to believe that one or more important parameters are still missing from the model, despite the fact that all of the obvious physical parts have been included. We have determined that one of these parameters is the force exerted by the strings on the bridge.

As noted by Conklin, the total force of the strings on a modern piano is approximately 200 kN, and the bearing force on the bridges is between one-half and 3 percent of the string force.[3] Thus, the total force on the bridges is in excess of 2000 N. Although this force is distributed along the length of the bridges, it is unlikely that a force of this magnitude will not have an effect on the motion of the soundboard.

To determine if the bearing force of the strings does indeed have a large enough effect on the frequencies and mode shape to account for the differences between the model and the experimentally derived shapes and frequencies, the tension of each string was reduced until the string lay slack. Once the strings were no longer exerting a force on the soundboard, the experiments described above were again performed. The resulting interferograms are shown in Figs. 4(e), 5(e), and 6(e), and the measured resonant frequencies are shown in the final column of Table II.

Comparing Fig. 4(d) with Fig. 4(e), and Fig. 5(d) with Fig. 5(e) indicates that the finite-element computer model of the soundboard predicts the mode shapes and resonant frequencies quite well, as long as there is no significant pressure exerted by the strings. From this we may conclude that, although work on experiments and modeling that has been reported in the literature has largely ignored the pressure of the strings on the soundboard, it does have a significant effect on the mode shape and resonant frequencies of the lowest modes.

It is not clear, however, that the force due to the strings has a significant impact on the deflection shapes at higher frequencies. This can be seen by comparing the interferograms shown in Fig. 3, made with the strings at full tension, with those in Fig. 7, which were obtained with the soundboard vibrating at the same frequencies after the strings had been removed. The similarity of the interferograms indicates that the effects of the string force on the deflection shape is not as important at higher frequencies as it is at the lower frequencies.

Eliminating the pressure on the bridges due to the strings does have a significant effect on the shape and frequency of the third mode, but the mode shape predicted by the model still does not agree well with the interferogram of this mode. Currently, we do not know why there is such poor agreement between the model and the experiment for the frequency and shape of the third mode.

It is interesting to note that once the pressure of the strings is removed from the soundboard, the effects of the individual ribs becomes apparent at low frequencies. Note, for example, that the node of the second mode is parallel to the side of the soundboard when the bridges are under the pressure exerted by the strings, but without this pressure the node follows the direction of the ribs. This indicates that the soundboard of a piano can be modeled as an isotropic plate at low frequencies only when the pressure due to the strings is present. Evidently, it is not only the ribs that compensate for the orthotropy of the wood at low frequencies, but the pressure placed on the bridges by the strings appears to also help in this regard.

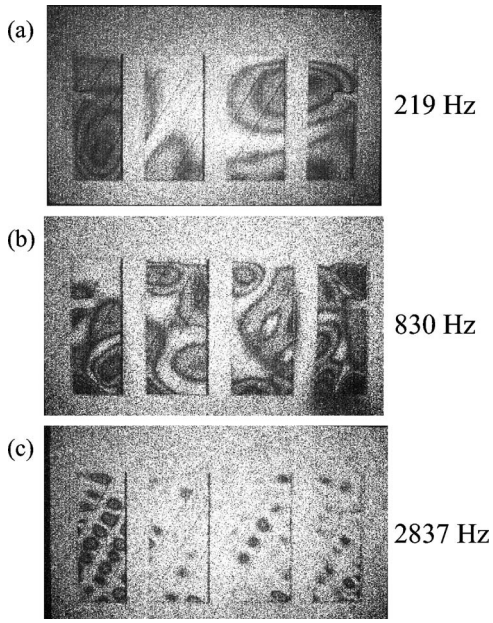

FIG. 7. Interferograms of the piano soundboard with the strings removed. The frequencies of vibration are the same as those in Fig. 3.

As noted above, at frequencies above those of the lower resonances, the pressure on the soundboard due to the strings appears to be less important. One reason for this may be that at higher frequencies the antinodes are small compared to the size of the soundboard, and except for the antinodes very near the bridges, the effect of the pressure on the bridge is unimportant.

In closing we note that, while the discussion above deals almost exclusively with the lowest two modes of the soundboard, the motion of the soundboard at these frequencies is extremely important in determining the overall tonal quality of the sound. For example, the asymmetry in the second mode, evident in Fig. 5(a), reduces the efficiency of acoustic short-circuiting between the two antinodes. This causes the lower frequencies to be radiated more efficiently than would be possible with a completely symmetric mode shape.

B. Comparison of the vibrational patterns of an acoustically driven and a point-driven soundboard

Although the deflection shapes of the soundboard are dependent only upon frequency when driven by a distributed acoustic signal, they can vary significantly when driven mechanically at a specific point. Since several resonances may be excited at any frequency, the position of the excitation will determine which resonances will be most efficiently excited. Therefore, excitation may occur at a node of a mode at one point but at an antinode at another, leading to the fact that the point of excitation will determine the deflection shape to a great extent.

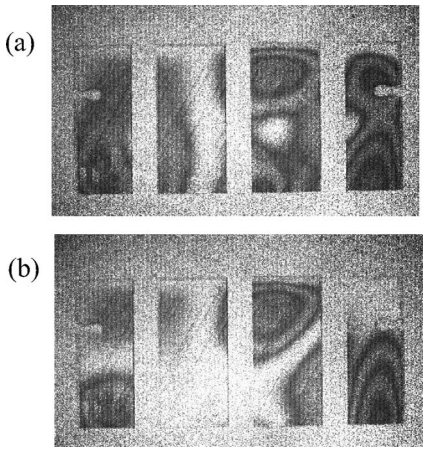

FIG. 8. Interferograms of the soundboard (a) when driven at a point on the bridge, and (b) when driven by a distributed acoustic source.

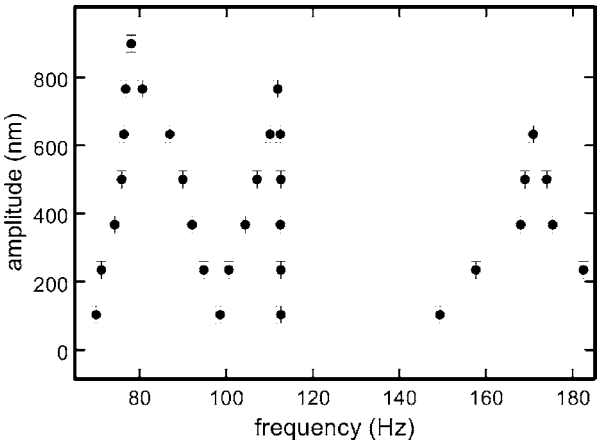

FIG. 9. Plot of amplitude of vibration vs frequency for the lowest three resonances of the piano soundboard.

To demonstrate the extent to which this can affect the deflection shape of the soundboard, an electromechanical shaker was placed so that it impacted the bridge near the terminating point of the C4 string on the treble bridge of the piano. Figure 8(a) shows the deflection shape of the soundboard when driven mechanically at a frequency of 328 Hz. For comparison Fig. 8(b) shows the deflection shape when the soundboard is driven acoustically at the same frequency by a speaker placed 2 m away. The difference between the two images in Fig. 8 leads one to ask if the shape of the bridge is actually designed to take advantage of the mode shapes of the soundboard.

Giordano has proposed that the shape of the bridge is designed to ensure that each string terminates near a location such that it cannot strongly excite a resonance in the soundboard at the fundamental frequency of the string.[4] This implies that each string terminates near a node in the soundboard, thus ensuring a slow transfer of energy to the soundboard from the string, and a commensurate lengthening of the decay time. We have investigated this conjecture by acoustically driving the motion of the soundboard at the fundamental frequency of each string using a speaker placed approximately 2 m away, and observing the deflection shape at the terminating point of the string associated with that frequency. In almost every case, the terminating point of the string lies extremely close to a node in the soundboard. Of all 88 strings, only the termination of the D5 string was not close to a node when the soundboard was driven at the fundamental frequency of the string. The termination of the D5 string was approximately midway between a node and antinode.

Preliminary experiments on other instruments indicate that not all pianos are designed so that the strings terminate near nodes in the soundboard at the fundamental frequency of vibration. Observations on a 6-ft. grand piano show that many of its strings terminate near antinodes.

C. Resonance measurements

Using the interferometer it is also possible to determine the resonance curve of the soundboard as long as a single antinode can be associated with an individual resonance. To do this it is only necessary to plot the amplitude of the deflection of one antinode of the mode as a function of frequency. Figure 9 contains such a plot of the lowest three modes of the soundboard without the strings.

The data shown in Fig. 9 were derived by driving the vibrations of the soundboard with a speaker placed approximately 2 m from the piano. The amplitude of the motion was determined using the interferometer as the driving frequency was varied. Using this technique it is possible to determine the frequency at which the modes begin to overlap significantly, thus setting an upper limit on modeling the soundboard as having individually isolated resonances. The data shown in Fig. 9 indicate that below approximately 200 Hz the modes are spaced widely enough to analyze them independently, although there is some overlap between the first and second modes far from resonance. Above this frequency the positions of the antinodes begin to shift noticeably with slight changes in frequency, indicating that there is significant overlap of the modes.

D. Measurement of the driving point impedance

The driving-point impedance determines much about the interaction of the string with the soundboard. It is defined as the driving force divided by the velocity, and to determine the driving-point impedance both of these quantities must be measured simultaneously. In the past, an impedance head that simultaneously measures the applied force and the acceleration has been used to determine the driving-point impedance; however, this arrangement has some disadvantages. The size and shape of these devices make it difficult to make measurements in the confined spaces of many pianos; therefore, only a limited number of measurements have been made on a fully assembled piano. Also, there have been reports of discrepancies in measurements that may be traceable to the construction and application of these devices.[1,6]

We have used an electronic speckle pattern interferometer to measure the driving-point impedance at several points on the soundboard, and at several different frequencies, without the use of an accelerometer. The interferometer was used to determine the velocity of the driving point while a shaker vibrated the soundboard at the point of interest. To measure

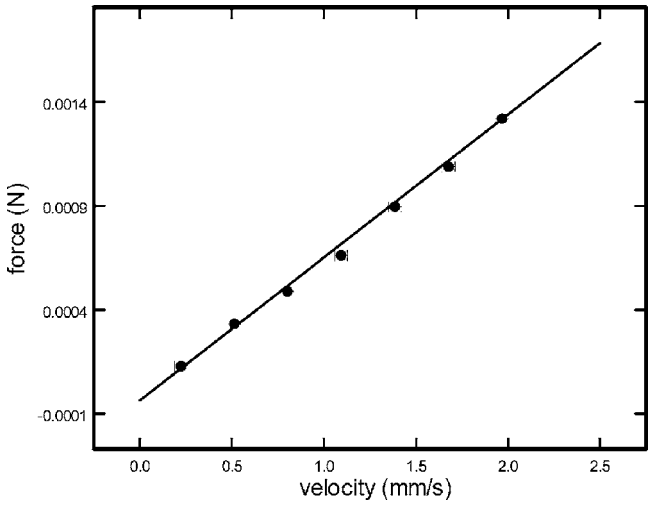

FIG. 10. Plot of the force vs velocity of a point on the treble bridge. The frequency of oscillation was 350 Hz. The slope of the graph is the driving-point impedance, which is 675±17 acoustic ohms.

the force applied to the soundboard, a force-dependent resistor was placed on the bridge at the point where the shaker touched it. An operational amplifier produced a voltage that was linearly proportional to the force exerted on the resistor.

Since the soundboard was driven harmonically at an angular frequency ω_0, the velocity of the driving point was given by

$$v = A_0\omega_0 \cos \omega_0 t, \tag{17}$$

where A_0 is the amplitude of the displacement. As the force was increased from zero, a black spot appeared at the position of the driving point when observed through the interferometer each time Eq. (14) was satisfied. This spot migrated into a ring as the driving amplitude was increased, and eventually a new spot appeared at the driving point. This process progressed until the limit of the driver was reached.

To determine the driving-point impedance, the force was measured each time the interferometry indicated that Eq. (14) was satisfied (i.e., a black spot appeared at the driving point as viewed through the interferometer). The force was plotted as a function of velocity, which was determined using Eq. (17), with A_0 determined from Eq. (14). The driving-point impedance is the slope of this graph, which was found by performing a linear regression. A typical graph of the force versus the velocity of the fully assembled soundboard is shown in Fig. 10. Each point is the result of three independent measurements of the displacement at the driving frequency. The uncertainty in the driving-point impedance is taken to be the uncertainty in the slope.

The advantages of this measurement system stem from the fact that the velocity is measured both directly and remotely. The remote measurement alleviates problems associated with the mass of an impedance head affecting the measurement of acceleration. Likewise, there are no resonances of the measuring system that can affect the results. Finally, this method provides an estimate of the uncertainty of the measurement, which is taken to be the uncertainty in the slope of the plot.

Before concluding this section, we note that the data presented here indicate that the approximations made in Sec. II are valid. Specifically, the linearity of the data used to determine the driving-point impedance, such as the example shown in Fig. 10, can only be possible if indeed the lines of equal displacement occur at the points determined by Eq. (14). Therefore, in the experimental arrangement described here, the assumptions that the functional form of Eq. (10) describes the movement of the soundboard and that $\epsilon \ll 1$ are valid. However, should an instance occur where these data are not linear, the value of ϵ could be determined simply by fitting the data to the equation $J_\epsilon(\xi)=0$, using ϵ as a fitting parameter.

V. CONCLUSIONS

We have described a method of electronic speckle pattern interferometry that not only works with moderate decorrelation of the speckle pattern, but demands it. We have shown theoretically and experimentally that this arrangement can be used to determine the deflection shapes of an object that is normally too unstable to observe interferometrically, and applied it to the study of a piano soundboard *in situ*.

Using this interferometer we have investigated the dynamics of the soundboard of a piano and have compared the results to a simple closed-form theory, as well as a finite-element model. Comparison of the deflection shapes of the piano to those predicted by these models demonstrates that the pressure exerted by the strings on the soundboard can make significant changes in mode shapes and resonant frequencies. The presence of this pressure has a significant effect on the lowest modes, but appears not to be important in determining the shapes and frequencies of the higher modes.

We have also shown that this interferometer can be used to determine resonance curves and driving-point impedance. We have presented the resonance curves for the lowest three modes of a soundboard and shown that they do not overlap significantly.

We close by noting that the applications of this interferometric technique are not restricted only to the investigation of piano soundboards. Harmonic vibrations of any unstable object that meets the requirements outlined in Sec. II can be observed using this technique. Additionally, the theory can be applied outside of the approximations if the value of ϵ in Eq. (10) is known.

ACKNOWLEDGMENTS

The authors thank B. Neller and M. Peterson for their generous support of this work. D. Parker assisted in the development of some of the computer models.

[1]K. Wogram, "Acoustical research on pianos. I. Vibrational characteristics of the soundboard," Das Musikinstrument **24**, 694–702 (1981).
[2]K. Wogram, "The strings and the soundboard," in *The Acoustics of the Piano*, edited by A. Askenfelt (Royal Swedish Academy of Music, Stockholm, 1990).
[3]H. A. Conklin, "Design and tone in the mechanoacoustic piano. II. Piano structure," J. Acoust. Soc. Am. **100**, 695–707 (1996).
[4]N. Giordano, "Simple model of a piano soundboard," J. Acoust. Soc. Am. **102**, 1159–1168 (1997).
[5]N. Giordano, "Sound production by a vibrating piano soundboard: Experi-

ment," J. Acoust. Soc. Am. **104**, 1648–1653 (1998).
[6]N. Giordano, "Mechanical impedance of a piano soundboard," J. Acoust. Soc. Am. **103**, 2128–2133 (1998).
[7]H. Suzuki, "Vibration and sound radiation of a piano soundboard," J. Acoust. Soc. Am. **80**, 1573–1582 (1986).
[8]J. Berthaut, M. Ichchou, and L. Jézéquel, "Piano soundboard: Structural behavior, numerical and experimental study in the modal range," Appl. Acoust. **64**, 1113–1136 (2003).
[9]J. Skala, "The piano soundboard behavior in relation with its mechanical admittance," in *Proc. of Stockholm Music Acoustics Conference (SMAC 03)*, 6–9 August, Royal Institute of Technology (KTH) (Royal Institute of Technology, Stockholm, 2003), pp. 171–174.
[10]E. J. Hansen, I. Bork, and T. D. Rossing, "Relating the radiated piano sound field to the vibrational modes of the soundboard," J. Acoust. Soc. Am. **114**, 2383 (2003).
[11]J. Kindel and I. Wang, "Modal analysis and finite element analysis of a piano soundboard," in *Proc. of 5th International Modal Analysis Conference*, 6–9 April, Imperial College of Science and Technology, London (Union College, Schenectady, NY, 1987), pp. 1545–1549.
[12]T. R. Moore, "A simple design for an electronic speckle pattern interferometer," Am. J. Phys. **72**, 1380 (2004).
[13]T. R. Moore, "Erratum: A simple design for an electronic speckle pattern interferometer," Am. J. Phys. **73**, 189 (2004).
[14]M. Abramowitz and I. A. Stegun, *Handbook of Mathematical Functions* (Dover, New York, NY, 1972).
[15]A. Leissa, *Vibrations of Plates* (Acoustical Society of America, Melville, NY, 1993).
[16]V. V. Bolotin, B. P. Makarov, G. V. Mishenkov, and Y. Y. Shveiko, "Asymptotic method of investigating the natural frequency spectrum of elastic plates," Raschetna Prochnost, Mashgiz **6**, 231–253 (1960).
[17]*Wood Handbook* (University Press of the Pacific, Honolulu, HI, 1974).